Suppressing Open Stopband for Terahertz Periodic Microstrip Leaky-wave Antennas

Thomas Haddad[1], Carlos Biurrun-Quel[2], Peng Lu[1], Hacer Kaya[1], Israa Mohammad[1], Andreas Stöhr[1]
[1] Department of Optoelectronics, University of Duisburg-Essen, Duisburg, Germany, thomas.haddad@uni-due.de
[2] Antenna Group. Public University of Navarra, Pamplona, Spain, carlos.biurrun@unavarra.es

***Abstract*—This paper reports on a periodic microstrip Leaky-wave antenna (LWA). The open stopband issue is suppressed by altering the unit cell using a matching stub. The developed LWA is based on a grounded InP-substrate of 50 µm and has been fabricated and characterized between 0.23 to 0.33 THz. The dispersion diagram of the designed unit cell shows enhancement of the attenuation constant at the broadside frequency of 0.273 THz and about 50% less deflection at the broadside region on the Bloch impedance curves, consequently better impedance matching at the input. The simulated scattering parameters of the proposed LWA show that the return loss S_{11} is below 17 dB except for the broadside, which has a value of 13.8 dB. Furthermore, the beam steering capabilities of the antenna are simulated in the WR3.4 band and confirmed experimentally between 0.26 and 0.33 THz proving the beam direction to steer from −12° to +33°, respectively.**

***Index Terms*—antennas, periodic leaky-wave antenna, open stopband, terahertz.**

I. INTRODUCTION

Leaky-wave antennas (LWAs) are a class of traveling wave antennas that leak power in a controlled manner while propagating through an altered guiding structure like a transmission line or a waveguide [1]. This time-dependent power leakage gives the LWAs a distinctive natural feature of adjusting the beam direction by tuning the operating frequency [1, 2]. Moreover, the LWAs are typically constructed as a single guiding structure, enabling low-complex feeding networks and reaching higher gains by enlarging the structure, which contributes to low-cost chips based on standard fabrication processes. The aforementioned features of the LWAs have promoted further research on developing these antennas for THz applications, such as radar [3, 4], 6G, and mobile THz communication [5-7].

LWAs radiate the fast wave, which means the phase constant β is smaller than the wavenumber k_0. The complex propagation constant $\gamma = \alpha + j\beta$, where α is the attenuation constant, which expresses the loss experienced by the signal while propagating through the unit cell in forms of radiation and losses in the material, i.e., $\alpha = \alpha_{rad} + \alpha_{loss}$ (ideally $\alpha_{loss} = 0$) [1]. The constant γ is usually indicated using the dispersion diagram of the leaking structure, where the transfer from a slow wave region to a fast one is defined by the "light line" $\beta = k = 2\pi/\lambda_0$, λ_0 is the wavelength. Whereas the ability of the unit cell to leak the power is carried on α, the frequency-dependent phase constant, $\beta(\omega)$, $\omega = 2\pi \cdot f$, essentially indicates the beam direction θ of the LWA, following [1, 8]:

$$\theta = \arcsin\left(\frac{\beta(\omega)}{k_0}\right) = \arcsin\left(\frac{c \cdot \beta(\omega)}{\omega}\right) \quad (1)$$

where c is the speed of light.

The periodic LWAs have a guiding structure that supports a slow wave (non-radiating mode) altered periodically in the form of replicated unit cell m-times with a periodicity of p using slots or stubs to enable the radiative mode through these discontinuities [1]. The periodically loaded guiding structure creates a Floquet wave, which consists of infinite space harmonics. The $n = -1$ space harmonic can fulfill the radiation condition [1]:

$$-k_0 < \beta_{-1} < k_0. \quad (2)$$

Although the periodic LWAs provide beam scanning capabilities from the backward quadrant to the frontward quadrant [1], they suffer a common issue: the open-stop band (OSB), consisting of a significant reduction of the antenna's gain when radiating at the broadside. This is caused by the contra-directional coupling of space harmonics, which leads to a significantly suppressed radiation power, i.e., low value for α_{rad} [1, 9]. In [10], some techniques were reported to handle the issue of the OSB for 1-D periodic LWAs. In this work, we will apply the technique of adding a matching stub to the unit cell to break the symmetry and enhance the radiated power on the THz periodic microstrip LWA, which was reported in [11].

II. CHIP DESIGN

A. Design of a Unit Cell

The unit cell of a periodic microstrip LWA can be designed following the formulas in [11]. The thickness of the substrate is 50 µm to reduce the number of surface-wave modes to the TM0 mode for a higher radiation efficiency [12] and to enable future integration with THz photodiodes. The layout of the proposed unit cell containing the matched stub is shown in Fig. 1, and the main dimensions are provided in Table 1. The dispersion diagram in Fig. 2a shows a comparison between the periodic LWA affected by the OSB (without the matching stub) and our OSB-suppressed LWA (with the matching stub). In both cases, it can be seen that the designed antenna is capable of producing a fast wave and scanning below the light line from 0.224 to 0.372 THz.

TABLE 1 PARAMETERS OF AN LWA UNIT CELL.

Dimension	Value	Dimension	Value
Length of the unit cell (period), p	353 μm	Matching stub width, w_{match}	20 μm
Width of the unit cell, w_{unit_cell}	1000 μm	Matching stub length, l_{match}	90 μm
Strip width, w_{strip}	70 μm	Position matching stub, O_{in}	30 μm
Stub width, w_{stub}	50 μm	Position 1st stub, O_{stub1}	58.25 μm
Stub length, l_{stub}	140 μm	Position 2nd stub, O_{stub2}	151.5 μm

On the one hand, the phase constant β is similar in both cases. On the other hand, the attenuation constant changes the behavior at the broadside region (around 0.273 THz), showing an increased value (solid blue curve) compared with the reduction in the fundamental antenna (the dotted blue line).

Another interesting comparison is given in Fig. 2b, where the simulated Bloch impedance is provided. The influence of altering the unit cell with a matching element reduced the curve deflection at the broadside frequency by almost 50%, which should lead to better impedance matching at the input, enhanced performance and radiation on the broadside direction.

B. Design of LWA

We used 20-unit cells to form the LWA (compared with 16-unit cells in [11]). This increment will enhance the directivity and the gain. The proposed antenna design is simulated and analyzed using the full-wave commercial electromagnetics (EM) solver Dassault Systems CST Studio 2021. The S-parameters of the LWA with suppressed OSB are provided in Fig. 3. (solid curves). By introducing the matching stub in the unit cell, the longitudinal symmetry is broken, i.e., $S_{11} \neq S_{22}$. The return loss S_{11} is overall below 17 dB, except for the broadside frequency of 0.273 THz, where it gets beyond 13.8 dB as the worst value. The degradation of S_{22} at the broadside frequency zone shows that the functionality of the matching stubs is applied only in one direction, but still better than the absence of the matching stubs (dotted S_{11} curve). Furthermore, the average value of the insertion loss is ~14 dB, which is about 3.8 dB better than the LWA with the issue of OSB, because the new structure is expanded by 4 extra unit cells.

III. CHARACTERIZATION OF THE LWA

A. Scattering Parameters

A CPW-to-microstrip transition was included in the fabricated structures, allowing the characterization of the scattering matrices. The scattering parameters were measured using a ZVA40 Vector Network Analyser (VNA) and a pair of waveguide extenders: a transceiver Rohde & Schwarz ZC330 (Tx/Rx) and a receiver (Rx) module Rohde

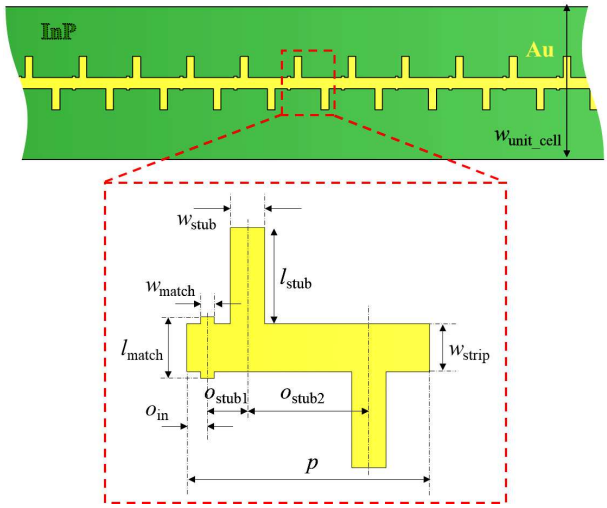

Fig. 1 Dimensions of a single unit cell, and line up the unit cells to form the body of the LWA.

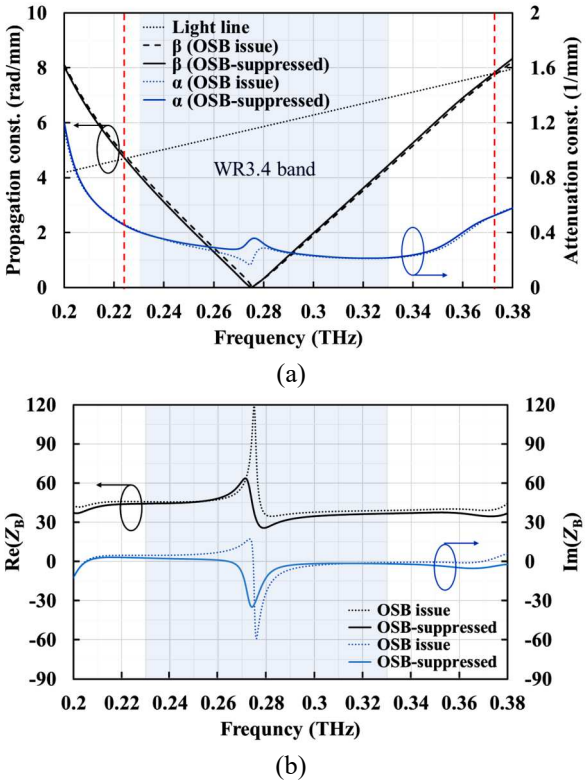

Fig. 2 (a) Simulated dispersion diagram of an LWA unit cell between 0.2 and 0.38 THz. (b) Bloch impedance of the proposed unit cell.

& Schwarz ZRX330. A TRL calibration kit [13] was fabricated to de-embed the transitions as well as the effect of the probes employed in the measurement. The de-embedded measurements were then compared to the simulated devices after applying a TRL algorithm to the simulated data.

The measured and simulated S-parameters of the de-embedded transition between 0.23 THz and 0.33 THz are presented in Fig. 4. The ripples in the measured S-parameters are likely caused by an irreversible effect of internal

reflections at one of the two probes used for the characterization. High values are noted in the simulated losses at 0.255 THz, which can be explained as follows: at 0.255 THz, the transition shows a strong resonance, which acts as an antenna with a very low transmission coefficient between the ports. This effect is noticed in the simulations of each TRL standard and provokes the TRL algorithm not to converge at such frequency points. On the other hand, the losses in the measurement setup before de-embedding helped in limiting the relevance of this phenomenon and allowed the de-embedding algorithm to converge. As well, the different probe positioning when measuring each TRL standard and device would include phase differences that reduced the relevance of this effect. However, this could not be reproduced in simulation. Nevertheless, a very good agreement is well observed overall despite this artifact.

B. 1-D THz Beam steering

The 1-D beam steering capabilities are simulated using CST by changing the frequency of the input using discrete port. The simulated far-field radiation patterns between 0.23 and 0.33 THz are presented in the polar diagram in Fig. 8. The beam scans from -50° at 0.23 THz to 42° at 0.33 THz and approaching the broadside direction at 0.273 THz.

The simulated realized gain of the LWA is demonstrated in Fig. 5 showing almost a constant value of 13.7 dBi in the WR3.4 band, including the broadside. The beam angle and the realized gain at 224.4 GHz are -63° and 11 dBi, respectively, whereas at 372.2 GHz the beam angle is 90° and the realized gain is 9.37 dBi covering a total beam steering range of 153°.

For a quantitative comparison, the beam direction and the 3-dB beamwidth for the LWA are provided in Fig. 6. The beam direction shows an excellent agreement between the measurements and the simulation. On the other hand, the beamwidth of the fabricated LWA is wider, which can be explained by the difference in the material of fabricated InP compared with the ideal one in the simulation.

The polar diagram of the characterized LWA at WR3.4 band is given in Fig. 7. The system setup restricted the measurement for the frequencies between 0.26 to 0.33 THz. Although, the simulated far-field at 0.273 THz showed an optimal performance, the characterized far-field was about 3 dB lower.

IV. CONCLUSIONS

This paper presented a periodic microstrip Leaky-wave antenna (LWA) with suppressed OSB using a matching stub in the unit cell. The dispersion diagram of the altered unit cell has an enhanced attenuation constant at the broadside frequency of 0.273 THz. The Bloch impedance has also been simulated, showing more stability of the impedance at the broadside frequency.

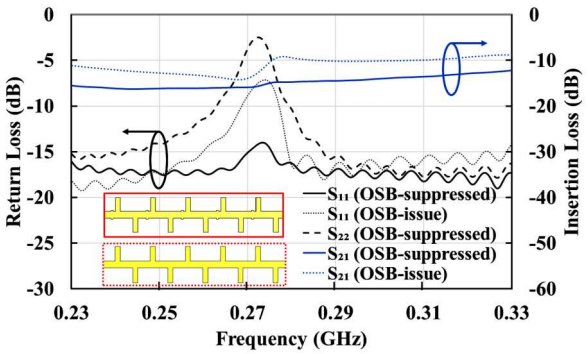

Fig. 3 Simulated S-parameters of an LWA with suppressed OSB and 20-unit cells (part of the LWA in the inset with solid frame) compared with the S-parameters of an LWA with OSB issue [11], which constructed from 16-unit cells (part of the LWA in the inset with dotted frame).

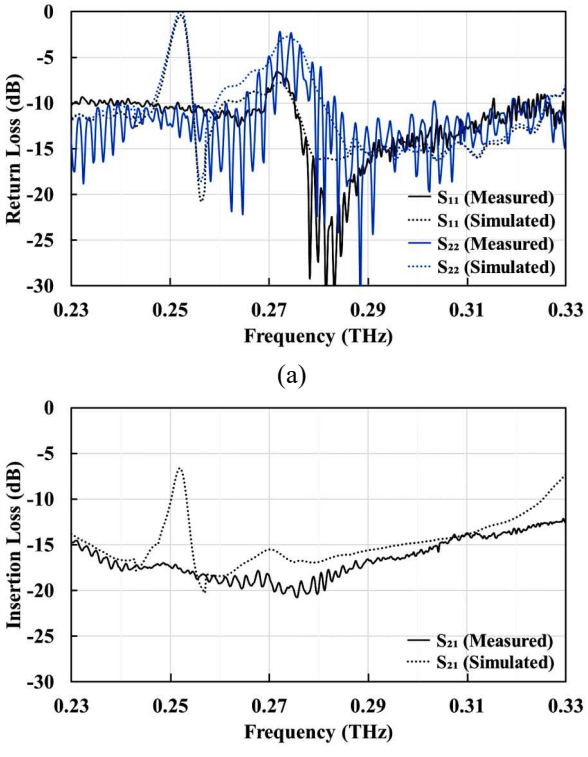

Fig. 4 (a) The measured return loss for a de-embedded LWA (solid curves) compared with the return loss of a de-embedded simulated structure (dotted curves). (b) The measured and simulated insertion loss for a de-embedded LWA.

The simulated return loss of the designed LWA is below 17 dB, except for the broadside, which has a value of 13.8 dB. Muchmore, the insertion loss ranges between 12.5 dB and 16.3 dB in the whole WR3.4. On the other hand, the characterized LWA approached worse scattering parameters affected by the non-ideal CPW-to-microstrip transition and the measurement setup.

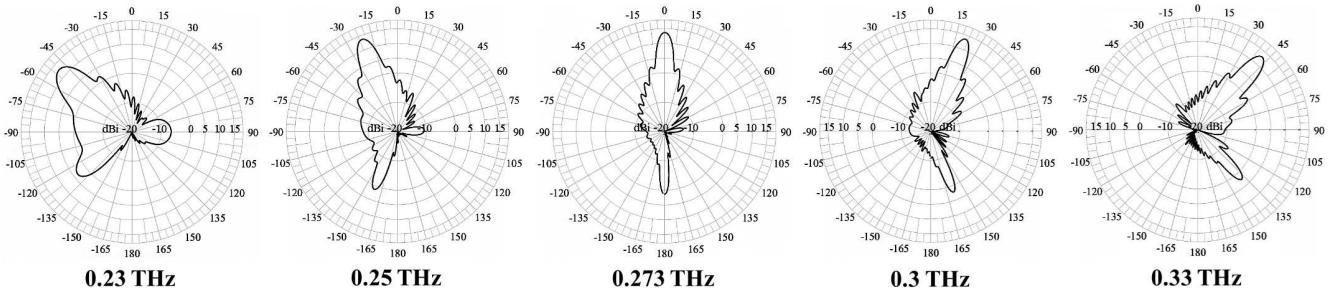

Fig. 8 Polar diagram of the simulated far-field radiation patterns of the LWA in H-plane for frequencies in WR3.4 band.

Simulated and characterized beam steering capabilities were introduced. A simulated beam steering range of 92° is obtained in the WR3.4 band when changing the frequency from 0.23 to 0.33 THz. Due to the limitation of the measurement setup, the steering range is experimentally confirmed from -12° at 0.26 THz to 33° at 0.33 THz. Furthermore, the beam direction and the 3-dB beamwidth of simulated and measured radiation patterns were examined for quantitative comparison perspectives.

ACKNOWLEDGMENT

The authors acknowledge financial support by the Deutsche Forschungsgemeinschaft (Project-ID 287022738–CRC/TRR 196(Project C07 and C06)) and Federal Ministry of Education and Research within the projects “Open6GHub” (grant No.16KISK017) and “6GEM” (grant No.16KISK039).

The authors are grateful to Benedikt Sievert from Universität Diusburg-Essen, Germany, for the experimental THz scattering parameter measurements, and Christian Preuß from Universität Duisburg-Essen, Germany, for the cleaving of LWAs.

REFERENCES

[1] D. R. Jackson and A. A. Oliner, "Leaky-Wave Antennas," in *Modern antenna handbook*, C. A. Balanis Ed.: A John Wiley & Sons, inc., publication, 2008, pp. 325-367.

[2] W. W. Hansen, "Radiating electromagnetic wave guide," USA Patent Appl. 2.402.622, 1946.

[3] P. Liu, Y. Liu, T. Huang, Y. Lu, and X. Wang, "Decentralized automotive radar spectrum allocation to avoid mutual interference using reinforcement learning," *IEEE Transactions on Aerospace and Electronic Systems,* vol. 57, no. 1, pp. 190-205, 2020.

[4] K. Murano *et al.*, "Low-profile terahertz radar based on broadband leaky-wave beam steering," *IEEE Transactions on Terahertz Science and Technology,* vol. 7, no. 1, pp. 60-69, 2016.

[5] C. Chaccour, M. N. Soorki, W. Saad, M. Bennis, P. Popovski, and M. Debbah, "Seven defining features of terahertz (THz) wireless systems: A fellowship of communication and sensing," *IEEE Communications Surveys & Tutorials,* 2022.

[6] M. Z. Chowdhury, M. Shahjalal, S. Ahmed, and Y. M. Jang, "6G wireless communication systems: Applications, requirements, technologies, challenges, and research directions," *IEEE Open Journal of the Communications Society,* vol. 1, pp. 957-975, 2020.

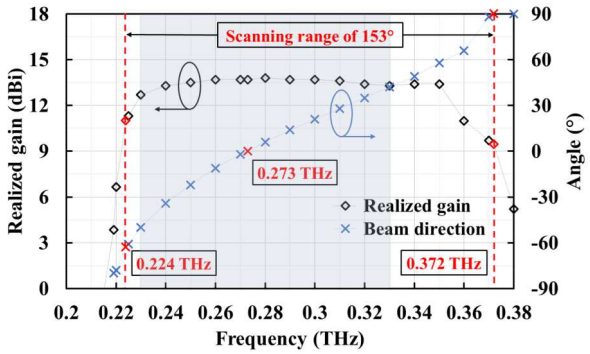

Fig. 5 Simulated realized gain and beam direction between 0.2 to 0.38 THz.

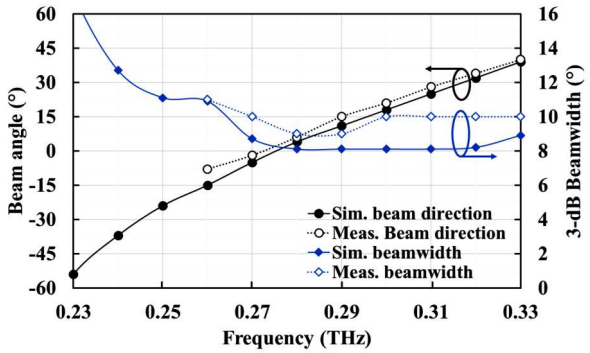

Fig. 6 Simulated and measured beam direction and 3-dB beamwidth from 0.23 to 0.33 THz of the microstrip periodic LWA.

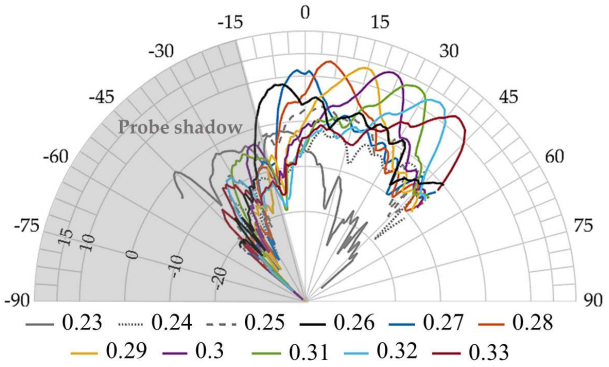

Fig. 7 Polar diagram of the characterized far-field for frequencies > 0.26 THz.

[7] P. Lu *et al.*, "Mobile THz communications using photonic assisted beam steering leaky-wave antennas," *Optics Express,* vol. 29, no. 14, pp. 21629-21638, 2021.

[8] C. Caloz, T. Itoh, and A. Rennings, "CRLH traveling-wave and resonant metamaterial antennas," *IEEE Antennas Propag. Mag.,* vol. 50, no. 5, pp. 25-39, 2008.

[9] P. Baccarelli, S. Paulotto, D. R. Jackson, and A. A. Oliner, "A new Brillouin dispersion diagram for 1-D periodic printed structures," *IEEE transactions on Microwave Theory and Techniques,* vol. 55, no. 7, pp. 1484-1495, 2007.

[10] S. Paulotto, P. Baccarelli, F. Frezza, D. R. Jackson, and Propagation, "A novel technique for open-stopband suppression in 1-D periodic printed leaky-wave antennas," *IEEE Transactions on Antennas and Propagation,* vol. 57, no. 7, pp. 1894-1906, 2009.

[11] P. Lu *et al.*, "InP-based THz beam steering leaky-wave antenna," *IEEE Transactions on Terahertz Science and Technology,* vol. 11, no. 2, pp. 218-230, 2020.

[12] D. Pozar, "Considerations for millimeter wave printed antennas," *IEEE Transactions on antennas and propagation,* vol. 31, no. 5, pp. 740-747, 1983.

[13] G. F. Engen and C. A. Hoer, "Thru-reflect-line: An improved technique for calibrating the dual six-port automatic network analyzer," *IEEE transactions on microwave theory and techniques,* vol. 27, no. 12, pp. 987-993, 1979.